Journal of Aerosol Science 127 (2019) 38–48

Contents lists available at ScienceDirect

Journal of Aerosol Science

journal homepage: www.elsevier.com/locate/jaerosci

Aerosolization and characterization of carbon nanotube and nanofiber materials: Relationship between aerosol properties and bulk density

Bon Ki Ku*, M. Eileen Birch

Centers for Disease Control and Prevention (CDC), National Institute for Occupational Safety and Health (NIOSH), Division of Applied Research and Technology (DART), 1090 Tusculum Ave, MS-R7, Cincinnati, OH 45226, USA

ARTICLE INFO

Keywords:
Aerosolization
Carbon nanotube
Acoustic generator
Fibrous nanomaterial

ABSTRACT

Potential inhalation of fibrous carbon nanomaterials depends on the manufacturing/handling process and their tendency for air dispersion. Because of the large variety of carbon nanotube and nanofiber (CNT and CNF) products, with varying physical and chemical properties, characterization of these materials and their associated exposure risks is challenging. In this study, we aerosolized different types of CNT and CNF materials using an acoustic generator (AG) and characterized their aerodynamic and physical properties. The generation characteristics of the AG for the different CNT and CNF materials were investigated by measuring aerosol number concentrations and its decay properties with time. Airborne particle properties such as mobility and aerodynamic diameters were measured using mobility and aerodynamic particle sizers. The bulk and effective densities of the powder and aerosol were obtained by measuring the mass and volume of the bulk material and aerosol particles, where effective density was calculated by a tandem mobility-mass technique. The relationship between the aerosol properties (i.e., particle size, concentration, and dustiness) and bulk density of the material was also investigated to understand the potential for dispersion in air. The results showed that the aerosol concentration decay for each nanomaterial has a unique time constant, and that the rate of decay is positively correlated with the bulk density of the powder: the lower the bulk density, the slower the concentration decay. The aerodynamic diameter increased with increasing bulk density, while the mobility diameter showed the opposite trend. In general, bulk density is smaller than the particle effective density, and the effective density tends to approach the bulk density as particle size increases. Also, the bulk density of the fibrous nanomaterials tested in this study showed a reasonable correlation with dustiness data obtained from both our measurements and the literature, which was relatively weak for non-fibrous powders. This study indicates that more loosely agglomerated CNT powders, with lower bulk densities, would be more readily dispersed, and the dispersed particles remain airborne for longer periods. Depending on particle size, such materials can pose higher exposure risks due to their ease of dispersion and longer residence times.

* Corresponding author.
E-mail address: bku@cdc.gov (B.K. Ku).

https://doi.org/10.1016/j.jaerosci.2018.10.004
Received 25 April 2018; Received in revised form 3 August 2018; Accepted 8 October 2018
Available online 19 October 2018
0021-8502/ Published by Elsevier Ltd.

1. Introduction

With increasing applications and global production of carbon nanomaterials, there has been concern about workplace exposure. The US National Institute for Occupational Safety and Health (NIOSH) has recommended a working lifetime exposure limit (1 μg/m^3, 8-h TWA, 45 years) to minimize the potential health risks associated with occupational exposure to carbon nanotubes and nanofibers (CNTs and CNFs) (NIOSH, 2013).

Although the use of these materials and products in the real world is much smaller than what the scientific community generally assumes (Stark, Stoessel, Wohlleben, & Hafner, 2015), characterization of their properties and exposure risks is still challenging, because of the large variety of CNT and CNF products, with varying chemical and physical properties (e.g., particles ranging from highly non-spherical fibrous structures to roughly spherical aggregates, all with low densities). Applications of CNTs include medical sensors, nanocomposite materials, electronic devices, thermoplastic additives, and biomedical science while applications of CNFs include coatings, composites and high-performance materials in energy conversion and storage such as lithium-ion batteries (Baughman, Zakhidov, & de Heer, 2002; Zhang, Aboagye, Kelkar, Lai, & Fong, 2014). Especially important with respect to the inhalation risks is their potential for dispersion in air. Bagging and dumping the manufactured powder in open areas, and cleaning powder containers were identified as activities that presented the greatest exposure risk at a facility manufacturing and processing CNFs (Birch, Ku, Evans, & Ruda-Eberenz, 2011; Evans, Ku, Birch, & Dunn, 2010).

The airborne behavior of CNT particles strongly depends on their aerodynamic properties and structure. From an exposure perspective, it is important to know the potential for air dispersion of a given material. Specifically, how many airborne particles (number-based concentration) are generated and/or how much (mass-based) CNT becomes airborne during a specific activity, and how long the generated aerosol could remain in the air. Evans and colleagues investigated elevated particle number and mass concentrations at a facility manufacturing and processing CNFs. They showed that the elevated mass concentrations of CNF aerosols generated during manufacturing can be relatively high, i.e., over 1 mg/m^3, and that the high concentrations are transient and process-dependent. It is hypothesized that the variation of the particle concentrations with time might depend on a material's physical properties such as particle size, shape, and bulk density. Concentrations also depend on the presence of local exhaust ventilation, and the overall facility design and ventilation system. To better understand the potential for air dispersion (e.g., during bagging and dumping CNTs) and exposure to different CNT materials in workplaces, i.e., what concentration levels of CNT materials could be expected to be generated, and how long will the materials remain airborne, it is necessary to examine the aerodynamic behavior of generated aerosols.

To aerosolize and characterize CNT materials, we used a pulsed acoustic aerosol generation system. Aerosol generation by acoustic vibration has been reported previously. McKinney, Chen, and Frazer (2009) used an acoustic generator to aerosolize a CNT material, and Weyel, Ellakkani, Alarie, and Karol (1984) aerosolized cotton dust using an acoustic generator that they developed. Schmoll, Elzey, Grassian, and O'Shaughnessy (2009) employed a generator similar to that of Weyel et al. to aerosolize a single-walled CNT (SWCNT) material. However, in these previous studies of CNTs (McKinney et al., 2009; Schmoll et al., 2009), aerosol generation was not investigated systematically for a variety of CNT materials with different aerosol properties. Therefore, it is important to investigate a variety of carbon nanomaterials to determine: 1) their potential for aerosolization, and 2) the residence times and size distributions of the generated aerosol particles.

The goal of this study is to investigate the aerosol generation characteristics of different carbon nanotube/nanofiber materials using an acoustic generator, and to characterize the aerodynamic and physical properties of the generated aerosols. Aerosols were characterized by measuring the number concentration and decay property with time. Also, airborne particle properties such as mobility and aerodynamic diameters, and bulk and effective density, were measured and compared. The relationship between the airborne properties and bulk density of the material is discussed.

2. Experimental methods

2.1. Nanomaterials

Seven different nanomaterials supplied by different manufacturers were examined in this study: one SWCNT, five multi-walled CNTs (MWCNTs), and a CNF material. These nanomaterials were chosen because they are (or were, in the case of Mitsui and Baytues) being manufactured in high volume and used globally. The CNano, Mitsui, NanoTechLabs, Baytubes and Nano Amor products are MWCNTs and were obtained from CNano (China), Mitsui (Japan), NanoTechLabs [NTL] (USA), Bayer MaterialScience AG (Germany), and Nanostructured & Amorphous Materials, Inc (Houston, TX), respectively. SWeNT is a SWCNT material that was produced by SouthWest Nanotechnologies (USA), and CNF is Pyrograf-III, produced by Applied Sciences Inc. (USA). The material and its physical properties are summarized in Table 1.

2.2. Experimental set up

Test aerosols of CNTs and CNFs were generated by an acoustic generator (AG), which is a custom PITT-3 type fluidized bed aerosol generator (AG-5025, Alburty Inc., Drexel, MO). This AG has been successfully used to generate test CNT aerosol for measurement of respirable and inhalable mass distributions and chemical analysis of the particles using cascade impactors and cyclones (Birch et al., 2018). The AG consists of a stainless steel vertical elutriator, latex diaphragm, and loud speaker. The elutriator section is fully enclosed and sealed with Teflon® gaskets. The generator is equipped with a separate module for air flow and audio control, with

Table 1
Names and physical properties of nanomaterials used in this study.

Material Manufacturer	Material model name	Tube OD[a] (nm), length (μm) and purity (%)	Specific surface area (m^2/g)
CNano	FloTube 9000	11, 10, 95 +	≥ 200[b]
Mitsui	Mitsui 7	40–90, 10–20, 95 +	22[c]
NanoTechLabs	NTL C-Grade	15, 100, 95	94[d]
SWeNT	SWeNT CG200	1.01, 1.02, 90 +	616[c]
Bayer	Baytubes C150P	13–16, 1- > 10, 95 +	196[d]
Nano Amor	MWCNT 1205YJ	10–20, 10–30, 95 +	146[c]
Applied Sciences, Inc.	Pyrograf- III CNF	60–100, NA, NA	41.1[e]

[a] OD stands for outer diameter. OD and purity are as listed by manufacturer.
[b] From the manufacturer data sheet.
[c] Birch, Ruda-Eberenz, Chai, Andrews, and Hatfield (2013).
[d] Zhao (2013).
[e] Ku (2010).

a frequency response of 30–3000 Hz. The audio signal to the speaker was controlled by a function generator (FG-8002, Goldstar, Korea) with a range of audio frequencies to vibrate the latex diaphragm, and a sine waveform was used in this study. A batch amount of test CNT powder (i.e., 0.2–0.5 g) was loaded on the center of the diaphragm. The aerosol flow was provided through the AG at 10 Lpm and was mixed and diluted with HEPA filtered air at about 20 Lpm. The diluted aerosol was supplied to a test chamber, where particle sampling was performed. The test chamber is a cylindrical metal bucket with an ID of 35 cm and height of 38 cm, and 16 sampling ports, as shown in Fig. 1. Before each test run, the test chamber was flushed with HEPA-filtered clean air, until the chamber background particle concentration dropped to a level well below 1–2 cm^{-3}, which was monitored with a condensation particle counter (CPC 3007, TSI Inc.).

Size distributions of the airborne particles in the chamber were measured continuously during the test by an aerodynamic particle sizer (APS 3321, TSI Inc.) with sizes ranging from 0.5 to 20 μm, and a scanning mobility particle sizer (SMPS, TSI Inc.) with sizes ranging from 10 to 650 nm at 5 Lpm and 0.3 Lpm, respectively. Total number concentration in the chamber was monitored by a CPC. Two CPCs were used to ensure that the particle concentration in the test chamber was uniformly distributed. Particle sampling was performed for one to two hours depending on aerosol concentration, to obtain characteristics of particle concentration decay in the test chamber as a function of time for a given batch amount of test material (typically, about 0.2 g). To investigate a relationship between particle concentration decay time and bulk density, bulk densities of all materials tested in this study were measured according to the WHO method A for measuring bulk density of powders in a graduated cylinder, except for the use of a small amount of powder (i.e., 0.05–0.2 g) (WHO, 2012) (see the following section details on measurement of bulk density). To determine an optimal acoustic vibrating condition for effective aerosolization of the CNT powders, the AG was tested for different vibrating modes (i.e., sweep or no sweep mode) with a given vibrating frequency (i.e., 60 Hz).

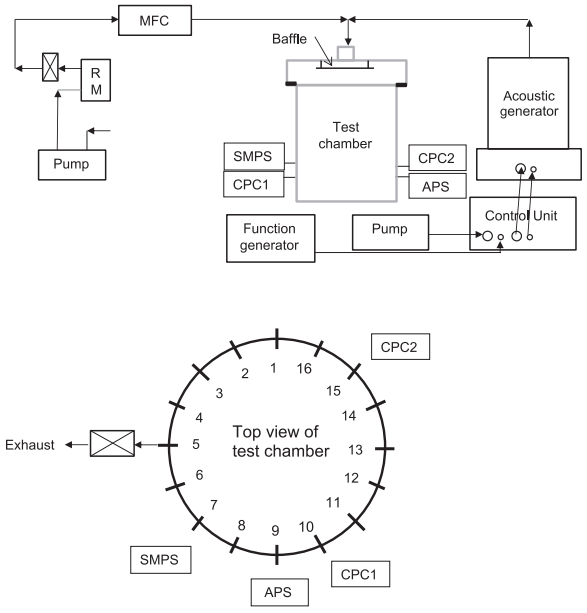

Fig. 1. Experimental setup for aerosol generation and schematic diagram of test chamber.

2.3. Measurement of bulk density of CNT powder

The bulk density of a powder is defined as the ratio of the mass of an untapped powder sample and its volume, including the contribution of the inter-particulate void volume (WHO, 2012). Thus, the bulk density depends on powder material density and spatial arrangement of particles in the powder. The bulk densities of seven nanomaterials used in this study were measured using the WHO method A (WHO, 2012). Briefly, a quantity of CNT material powder was poured through a sieve with apertures equal to 1.0 mm (sieve mesh # 18) to break up agglomerates that may have formed during storage. Below the sieve a funnel was mounted on a stand. The sieved powder was collected through the funnel into a graduated cylinder which was weighed with a microbalance in advance. Then, the freely settled apparent volume (V) was read to the nearest graduated unit and the cylinder with the sieved powder was weighed to obtain the mass (m) of the powder. The bulk density was determined by the mass divided by volume, and duplicate or triplicate measurements for each material were made and average bulk density and standard deviation (for triplicates) were calculated.

3. Results and discussion

3.1. Generation characteristics of the acoustic generator

Fig. S1 in the supplementary information (SI) shows the particle number concentration under different vibrating conditions for the AG. Fig. S1(a) shows the difference between number concentrations without frequency sweeping and with sweeping at a vibrating frequency of 60 Hz. Without sweeping, the number concentration was about 60 cm^{-3}, but when the sweeping was operated, it suddenly increased to 800 cm^{-3}, which corresponds to an increase in concentration by a factor of 13, indicating that vibrating the diaphragm with sweeping is much more efficient in aerosolizing CNT powder than with vibration alone. It is worth noting that for a given batch amount of the Nano Amor CNT (~0.5 g) material, the particle concentration was stable at a lower flow rate (1.3 Lpm) during the entire test period. The amount of dispersed aerosol was enough for the particle concentration to remain stable at the lower flow rate for about 75 min. A stable number concentration can be obtained, depending on the initial batch amount and aerosol flow rate. Fig. S1(b) & (c) show variation of number concentrations with different sweep widths at a low sweep rate, about one sweep per 3.5 s for two CNT materials. Sweep rate means how often the frequency sweep reiterates, and sweep width is the range of frequencies that are traversed with each sweep. As the sweep width increased, the number concentration increased at a given frequency of 60 Hz. The effect of sweep width on the number concentration was in the range of a factor of about two for different sweep widths, which was relatively small compared to the difference seen with and without sweeping, as shown in Fig. S1(a). It is worth noting that the time required for stable concentrations fell in a range of about 3–5 min, depending on the tested materials, indicating that the test powder may be dispersed well during this time frame. Fig. S1(d) shows aerodynamic size distributions from Fig. S1(a), measured by APS under no sweep and with sweep. Acoustic vibration with sweeping decreased modal diameters of particle size distributions and increased particle number concentrations. This measurement confirms that the use of vibration with sweep improves aerosolization of CNT powders. Based on these results, the conditions of 1/2 sweep width at a low sweep rate, at 60 Hz, was used for all experiments in this study.

To characterize the particles aerosolized by the AG, number concentration, aerodynamic (d_{ae}) and mobility size (d_m) distributions were measured. The d_{ae} and d_m typically capture aerodynamic and diffusional characteristics of the particles in the submicron or micron size ranges, which is important to understand particle exposures and their potential health effects. Fig. S2(a) shows total number concentration of Nano Amor CNT material aerosolized by the AG during the test, measured by different real-time instruments (CPCs, APS, and SMPS). The number concentrations measured by two CPCs were intended to ensure that the airborne particles in the test chamber are uniformly distributed. The two CPC-measured number concentrations in Fig. S2(a) are found to be similar, within 5–15%, indicating the generated aerosol is well mixed in the test chamber. The concentrations measured by the APS and SMPS are lower than that measured by a CPC. This may be because the APS has a poor detection efficiency for particles below about 0.5 μm, and the SMPS had an impactor located prior to its inlet to exclude particles larger than about 1 μm. Fig. S2(b) & (c) show aerodynamic and mobility size distributions, respectively. Over time, the sampled number concentration decreased, but modal diameters of the distributions measured at different times during the test were similar; the modal diameters of aerodynamic and mobility distributions were about 2.1 μm and 70 nm, respectively, for the Nano Amor CNT material.

3.2. Time dependence and decay characteristics of particle concentration

The characteristics of decay of particle concentrations generated by the AG were measured for all seven nanomaterials tested in this study. Fig. 2 shows total number concentration aerosolized by the AG as a function of time. Different CNT materials showed distinct decay characteristics of the particle concentration. The decay time constant, τ, defined as time needed for the initial number concentration to decrease to a factor of 1/e (≅0.368) (e is the base of natural logarithm), was obtained by fitting number concentration data to an exponential decay function. The Mitsui MWCNT has the largest time constant (i.e., 108.3 min) and Baytube MWCNT has the smallest one (2.7 min). The decay time constant of SWeNT SWCNTs is about 10.9 min, while that of the CNFs is about 22.1 min. The other CNano, Nano Amor, and NTL MWCNT materials have 5.5 min, 6.4 min, and 8.1 min, respectively. The larger the decay time constant is, the more slowly the particle concentration decays. It is hypothesized that the particle aerosolization and decay characteristics of all the CNT materials may depend on their physical properties (i.e., bulk density) at a given aerosol flow rate through the AG, and this dependence is discussed in the following section. It is worth noting that the regression parameter, R^2,

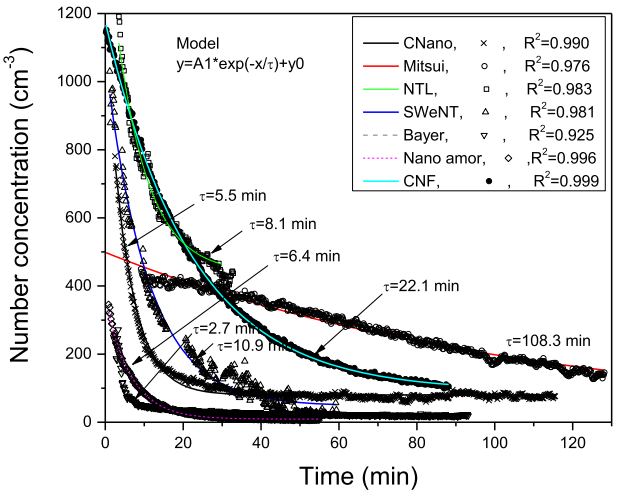

Fig. 2. Number concentration as a function of time for different carbon nanotube materials. Initial batch amount is 0.2 g for all materials except Baytubes (0.5 g). Frequency was 60 Hz with low-rate sweeping (about one sweep per 3.5 s) of the acoustic generator.

ranges from 0.925 to 0.999, indicating that the fitted data follows the exponential decay well.

3.3. Dependence of particle aerosolization and decay on particle bulk properties

To investigate relationship between the decay characteristic and bulk density of the material, we measured the particle bulk density using the WHO method (WHO, 2012). Table 2 summarizes the decay time constant and bulk density for each material. The Mitsui CNT, having the lowest bulk density (0.0066 g cm^{-3}), shows the slowest decay of the concentration, i.e., largest decay time constant, while the Baytube CNT (0.15 g cm^{-3}) presents the fastest decay characteristics. When handling the materials in a laboratory hood, it was obvious that the Mitsui CNT was very fluffy, and it tended to fly away easily, while the Baytube CNT appeared relatively dense. The bulk density of the Mitsui was found to be about two orders of magnitude lower than that of the Baytubes. In addition to the large difference in their bulk densities, the Mitsui and Baytube CNTs showed a difference in the decay time constant, by a factor of 40. The CNF particles (0.036 g cm^{-3}) show fast decay in concentration relative to the Mitsui CNTs. Fig. 3 presents the decay time constant as a function of bulk density for the tested nanomaterials. It is clear that the bulk density of the powder affects the decay characteristic of the particle concentration. The decay time constant decreases with increasing bulk density, being approximately inversely proportional to bulk density. The functional correlation between the decay time constant and the bulk density is good, with a regression parameter R^2 of 0.997. Based on this finding, it is expected that the more loosely agglomerated a material is (i.e., the lower bulk density), the more easily particles could be aerosolized from the bulk powder, and the slower the decay of the particle concentration will be.

Fig. 4 shows typical SEM images of the airborne particles collected in the test chamber using an impactor with cutoff of 1.55 μm. SEM images confirm that the Mitsui particles have less agglomerated fibrous structure while the Baytube particles show a very compact structure. Also, CNano particles collected on the impactor are shown to be compact.

3.4. Aerodynamic and mobility diameters of aerosolized particles

Figs. S3 & S4 show typical aerodynamic and mobility size distributions of the carbon nanotubes and nanofibers aerosolized by the

Table 2
Characteristic time for exponential decay of particle number concentrations generated by acoustic generator, and bulk density measured in this study according to the WHO method for measuring bulk density of powders.

Material	Characteristic time for exponential decay (min)	Bulk density (g cm^{-3})	[a]Bulk density (g cm^{-3})
CNano	5.5	0.0854 ± 0.0001	0.03–0.15
Mitsui	108.3	0.00663 ± 0.00003	–
NanoTechLabs	8.1	0.1110 ± 0.0058	–
SWeNT	10.9	0.0774 ± 0.0024	0.091
Bayer	2.7	0.1539 ± 0.0030	0.15–0.35
Nano Amor	6.4	0.09578 ± 0.00027	0.04–0.05
CNF	22.1	0.03645 ± 0.0015	0.016–0.048[b]

[a] As listed by the manufacturer.
[b] Converted from the values of 1–3 lb/ft^3. http://pyrografproducts.com/nanofiber.html.

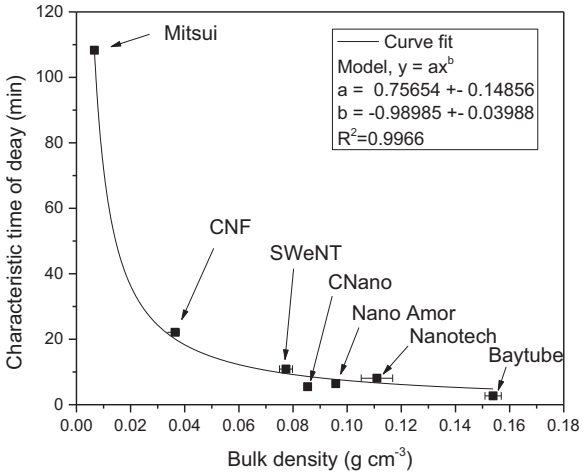

Fig. 3. Characteristic time of decay of number concentration as a function of bulk density measured by WHO method. The decay time constant is approximately inversely proportional to bulk density.

AG, respectively. Among the tested materials, Mitsui and CNF particles have lower modal aerodynamic diameters, and the particles from the CNano, Bayer, and Nano Amor have a similar modal diameter that occurs at around 2.0 μm, as shown in Fig. S3. The particles from the SWeNT SWCNT have a bit broader aerodynamic distribution, but with a similar modal diameter to those of the CNano, Bayer and Nano Amor materials, while the NTL CNTs show a bimodal distribution with major and minor modal diameters of about 1.8 μm and 1.0 μm, respectively. Fig. S4(a) & (b) show original and normalized mobility size distributions of CNTs and CNFs. There are several groups of mobility size distributions to be categorized in terms of modal diameter. Modal diameters of CNano, SWeNT, Bayer and Nano Amor CNTs are all below 100 nm, while those of Mitsui and CNF particles are above 100 nm. NTL particles have a modal diameter at around 100 nm and a broad distribution. The broad size distribution of the NTL particles in mobility diameter is expected because they have a bimodal distribution in aerodynamic diameter. According to the SEM morphology analysis, as NTL particle size decreased, the morphology of the particle became curved, resembling the shape of a macaroni noodle (Fig. 4b). Geometric mean diameters (GMDs) and geometric standard deviations (GSDs) for aerodynamic and mobility size distributions measured for the tested nanomaterials are summarized in Table 3. Mean aerodynamic and mobility diameters (d_{ae} and d_m) of the generated particles ranged from 0.79 to 2.10 μm, and from 63.8 to 317 nm, respectively. Geometric standard deviations for d_{ae} and d_m ranged from 1.37 to 1.58, and from 1.58 to 2.15, respectively.

We also investigated the effect of particle bulk density on aerodynamic and mobility diameters of particles aerosolized by the AG. Fig. 5 shows that aerodynamic diameter increases with increasing bulk density while mobility diameter decreases, following a reverse trend. The opposite trends for these two diameters could be explained based on their physical meaning. The aerodynamic diameter depends on a settling velocity, which is proportional to particle diameter squared and particle density, and electrical mobility diameter depends on particle electrical mobility defined as a migration velocity per unit electric field. Both the settling velocity and migration velocity in turn depend on particle drag related to particle morphology and structure. The settling velocity and the migration velocity increase with decreasing drag. As the bulk density increases, particles tend to become more compact. With the particle being more compact, the settling velocity and the migration velocity of the particle would increase due to relatively small drag compared to loosely agglomerated particles with high dynamic shape factor. Thus, the aerodynamic diameter would increase and the mobility diameter (this is inversely proportional to migration velocity) would decrease with decreasing drag. The result from Fig. 5 is consistent with this expectation.

It was found that mobility diameter decreased with increasing BET SSA for the nanomaterials tested in this study while aerodynamic diameter seemed to increase with BET SSA, as shown in Fig. S5. Compared to spherical particles, the mobility diameter of the CNT particles follows the relationship between mobility diameter and BET SSA for spherical particles, but the aerodynamic diameter of the CNT particles seems to show the opposite trend. The CNT particles with the same BET SSA as spherical particles had larger mobility diameters, indicating that the morphology of the CNT particles is clearly non-spherical. But the trend in the relationship (mobility diameter and SSA) indicates that the mobility diameter is related to physical diameter of particles. The ratio of the BET SSA of the CNT particles to spherical particles with same mobility diameter is about two to four. The difference between the two BET SSAs seems to increase as the mean mobility diameter decreases. Of note, the mobility and aerodynamic diameter do not change significantly as a function of BET SSA for values above 200 m^2/g. This may relate to a higher extent of agglomeration for CNT particles with BET SSA above 200 m^2/g.

3.5. Relation between particle effective density and bulk density

We examined how the bulk density would be correlated with particle effective density. The effective density of a particle was defined as mass divided by volume based on mobility diameter. The effective density defined in this way has been used to

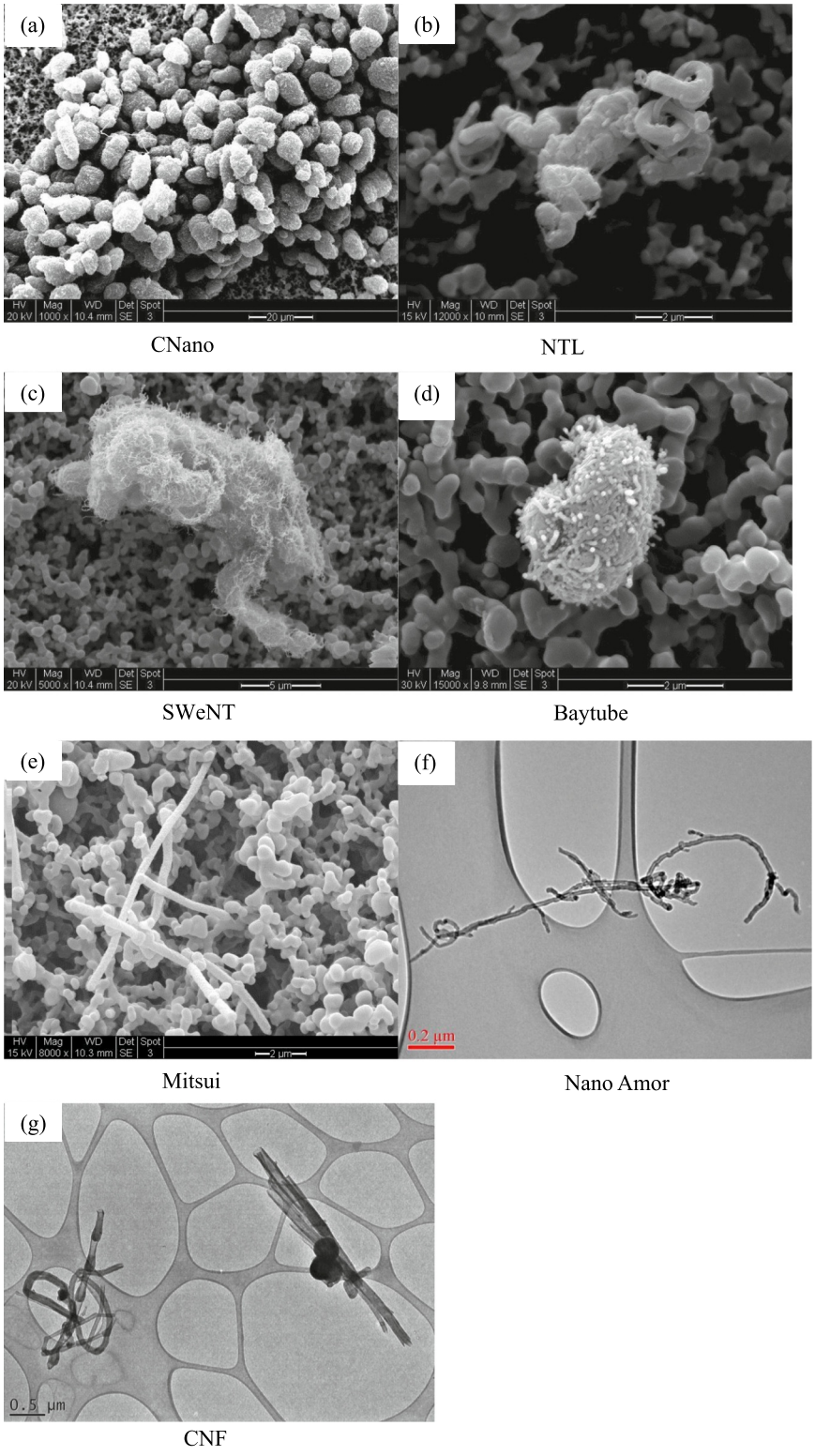

Fig. 4. SEM/TEM images of CNT particles collected on an impactor with cutoff of 1.55 μm. Nano Amor MWCNT and CNF particles [(f) & (g)] are for sizes (0.4 and 1.0 μm) in mobility diameter, respectively.

Table 3
Geometric mean diameters (GMDs) and geometric standard deviations (GSDs) for aerodynamic (d_{ae}) and mobility size (d_m) distributions measured by APS and SMPS, respectively.

Material	GMD (μm) for d_{ae}	GSD for d_{ae}	GMD (nm) for d_m	GSD for d_m
CNano	2.10	1.37	69.7	1.71
Mitsui	0.79	1.45	317.0	1.58
NanoTechLabs	1.35	1.58	137.2	2.15
SWeNT	1.89	1.46	63.8	1.87
Bayer	1.90	1.55	69.5	1.98
Nano Amor	2.09	1.41	78.2	1.95
CNF	1.02	1.58	235.4	1.99

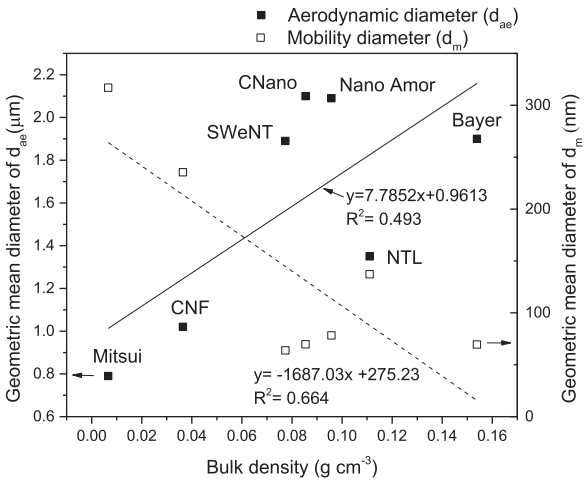

Fig. 5. Aerodynamic and mobility diameters (d_{ae} and d_m) as a function of bulk density measured by WHO method.

characterize the structure of different types of particles such as diesel exhaust, atmospheric particles, and nanoparticles (Ku & Evans, 2012; Ku, Emery, Maynard, Stolzenburg, & McMurry, 2006; McMurry, Wang, Park, & Ehara, 2002; Park, Cao, Kittelson, & McMurry, 2003). In this study, CNano CNT was chosen to test the relationship between the bulk density and particle effective density. The effective density was obtained using a tandem mass-mobility technique (Ku et al., 2006). Briefly, particles were selected as single mobility particles by DMA and provided to an aerosol particle mass analyzer (APM, Kanomax Inc., New York, NJ) to measure the mass of the classified particles. For size classification, particles are balanced between electrical and centrifugal forces in the two concentric rotating cylinders of the APM. Their number concentration, downstream the APM, vs. the voltage applied to the cylinders is measured to obtain the average particle mass. Fig. S6 shows number concentration measured downstream as a function of APM voltage, and mass and effective density obtained from these measurements. The slope from a linear fit between mass and mobility diameter is a 'mass scaling factor' indicating particle structure. The CNano particles ranging from 70 nm to 200 nm in mobility diameter have mass scaling factor of 2.5. According to the recent study from Ku and Kulkarni (2015), various SWCNT and MWCNT particles have mass scaling factors in the range from 2.17 to 2.57, and thus, the CNano particles show a scaling factor close to the upper value found in the previous studies, indicating its relatively compact structure. Effective density of the CNano particles is in the range of 0.3–0.5 g cm^{-3}, showing its tendency of decreasing with increasing mobility diameter. Comparing the bulk density of the CNano material (i.e., 0.085 g cm^{-3}) with the effective density of the particles, the bulk density is less than the effective density. Considering that the bulk density accounts for larger agglomerated particles and interspace among the particles, the chances are high that bulk material has more porosity and void space than individual particles, especially smaller ones. As the effective density decreases with increasing particle size, as shown in Fig. S6 and in previous studies (Ku & Kulkarni, 2015; Ku et al., 2006), it is expected that the effective density of larger agglomerate particles will approach the bulk density with increasing particle size. Ku and Kulkarni (2015) measured effective densities of Nano Amor CNT particles generated by vortex shaking and showed that they decrease from about 0.6–0.2 g cm^{-3} as mobility diameter increases from 100 to 400 nm. The bulk density of Nano Amor material measured in our study is 0.096 g cm^{-3}, showing a tendency of the effective density to approach the bulk density. Ku et al. (2006) obtained effective densities of CNF particles, which ranged from 1.2 to 0.4 g cm^{-3}. This effective density is larger than the bulk density of CNF material (0.036 g cm^{-3}) measured in this study. It is worth noting that the bulk density of the CNF is one order of magnitude smaller than the effective density. This may be due to the fact that the large clumps of the CNF are fibrous and have open structure. Based on the data of the effective and bulk densities, it is concluded that the bulk density is in general smaller than the particle effective density, and the effective density tends to approach the bulk density as particle size increases.

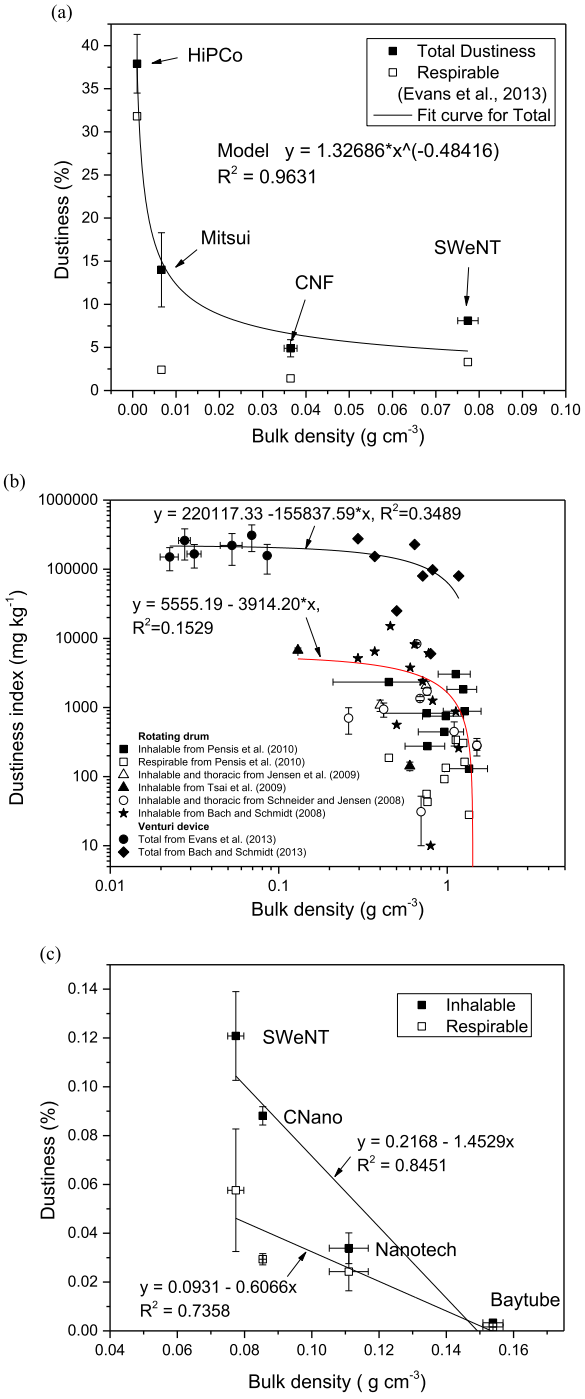

Fig. 6. (a) Dustiness vs. bulk density for CNT materials, (b) dustiness vs. bulk density for fine and coarse materials (from literature), (c) dustiness vs. bulk density for CNT materials is based on the mass determined using cascade impactors (this study). Dustiness data in (a) are from Evans et al. (2013). All bulk densities were measured (this study) except HiPCo SWCNTs, for which density was obtained from Maynard et al. (2004) and Baron et al. (2008). The fitting curve for the rotating drum was obtained with inhalable dustiness data only. The dustiness data in (c) were obtained (this study) by collection of materials using 8-stage Marple cascade impactors and determining the elemental carbon (EC) mass on each stage. The inhalable and respirable fractions of the total mass were calculated using the ICRP model (Hines, 1999). See text for details.

3.6. Relationship between bulk density and dustiness of nanomaterial powder

The tendency of a bulk nanomaterial (and other powders) to become airborne (i.e., its dustiness) is relevant to the potential inhalation exposure of workers that produce/process these materials. It is well known that the measured dustiness of a given

materials depends on test apparatus, and the prior conditioning (e.g., at a given humidity) and properties of the tested bulk material (BSI, 2013). In this section, the dustiness of nanomaterials as a function of powder bulk density is discussed, which is believed to be one of the most important material-specific parameters related to dustiness (BSI, 2013). The relationship between bulk density and dustiness of nanomaterial powder has not been investigated in detail to date.

Fig. 6(a) shows total (or inhalable) and respirable dustiness as a function of bulk density for four of the nanomaterials tested in this study. The values of the dustiness, defined as a ratio of airborne mass collected on a filter to initial batch amount of the material powder (in percentage), were obtained from Evans, Turkevich, Roettgers, Deye, and Baron (2013), who used the same products tested in this study. All the materials are fibrous and have relatively low bulk densities ranging from ~0.001 (HiPCo SWCNT) to 0.077 g cm^{-3} (SWeNT) which were measured in our study except for HiPCo, whose bulk density was obtained from two independent studies (Baron et al., 2008; Maynard et al., 2004). Total and respirable dustiness decrease as the material bulk density increases for these particular carbon nanotubes and nanofiber materials, and good correlation between the total dustiness and bulk density was found. The correlation value, R^2, is 0.96. To investigate if there exists a similar correlation for a wide range of materials such as metal oxides and other dusts, including fine and coarse particle materials with non-fibrous morphologies, dustiness data collected using a rotating drum and venturi device were obtained from the literature (Bach & Schmidt, 2008; Evans et al., 2013; Jensen, Koponen, Clausen, & Schneider, 2009; Pensis, Mareels, Dahmann, & Mark, 2010; Schneider & Jensen, 2008; Tsai et al., 2009). Fig. 6(b) shows two groups of dustiness data: one from a rotating drum test and the other from a venturi dispersion test. The data from the venturi dispersion include fumed metal oxides such as silica and titania, and the data from the rotating drum test are for metal oxides, clay, talc and silica dust. The dustiness index on the y-axis in Fig. 6(b) was expressed as the quantity of dust collected (mg) divided by the mass (kg) of the initial batch amount of the material tested. The bulk densities of some materials (i.e., SiO_2 Aerosil, TiO_2 Aeroxide P25, and Printex 90 carbon black) used in the venturi test (Evans et al., 2013) were measured in our study using the WHO method A (WHO, 2012). In general, dustiness decreases with increasing bulk density. The correlation between the dustiness and bulk density is somewhat weak for both groups, whose R^2 is 0.153 and 0.349, respectively. The data from the venturi dispersion test shows slightly better correlation with bulk density than those from the rotating drum test. This may be due to the fact that the venturi device uses a more energetic dispersion process (Evans et al., 2013), which may generate more particles from a material with a lower bulk density than does the rotating drum. It is worth noting that most data from the literature are for powders with bulk densities in the range from 0.1 to 1.5 g cm^{-3}, particularly for the data from the rotating drum test, while our data in Fig. 6(a) are for powders with densities lower than 0.1 g cm^{-3}. To confirm the positive correlation between dustiness and bulk density for fibrous carbon nanomaterials, as shown in Fig. 6(a), we collected samples of the materials using 8-stage, Marple cascade impactors (Model 298, Tisch Environmental, Inc., Cleves, Ohio) in the test chamber and measured the mass of elemental carbon (EC) on each stage of the cascade impactor by NIOSH Manual of Analytical Method (NMAM) 5040, which quantifies organic and elemental carbon (OC and EC) on quartz filters. Then, we calculated inhalable and respirable fractions of the sample using the ICRP model (Hinds, 1999). Fig. 6(c) shows inhalable and respirable dustiness results obtained from the cascade impactor data as a function of bulk density for four CNT materials. Both inhalable and respirable dustiness values have similar correlations with bulk density. The dustiness decreases with increasing bulk density, confirming the result from Fig. 6(a). The regression values for the dustiness vs. bulk density are 0.85 and 0.74, respectively. These values are a bit smaller than those for the dustiness from the venturi device, but results clearly show the tendency of dustiness to decrease with bulk density. Based on these two independent results, from Fig. 6(a) & (c), and the literature data [Fig. 6(b)], it is concluded that the correlation between dustiness and bulk density tends to be strong for fibrous nanomaterials but may be relatively weak for fine and coarse materials without fibrous structures. However, further research needs to be done to investigate the effect of dustiness test systems (i.e., rotating drum and venturi device) on the potential correlation between dustiness and bulk density for a wide range of materials.

4. Conclusions

In this study, we aerosolized different types of carbon nanotube and nanofiber materials using an acoustic generator (AG) and characterized their aerodynamic and physical properties. The generation characteristics of the AG for the different nanomaterials were investigated by measuring number concentration and its decay property with time. Airborne particle properties such as mobility and aerodynamic diameters were measured using mobility and aerodynamic particle sizers, and bulk or effective density was obtained by measuring the mass and volume of the material or particle. The relationship between the airborne properties (i.e., concentration decay time, particle size and dustiness) and bulk density of the material was also investigated to understand the potential for dispersion in air. The results showed that the decay characteristic for each nanomaterial gives a unique decay time constant, and that the lower the bulk density is, the slower the concentration decay is. The aerodynamic diameter increased with increasing bulk density, while the mobility diameter represented the opposite trend. The bulk density is, in general, smaller than the particle effective density, and the effective density tends to approach the bulk density as particle size increases. It was found that the correlation between material dustiness and bulk density tends to be strong for fibrous nanomaterials and relatively weak for fine and coarse materials without fibrous structures. More loosely agglomerated CNT powders, with lower bulk densities, are expected to be more readily dispersed, and particles remain airborne for longer periods. Depending on particle size, such materials can pose higher exposure risks due to their ease of dispersion and longer residence times.

Acknowledgments

We thank Qi Zhao (University of Cincinnati) for assistance with sample preparation, and Aleks Stefaniak, Greg Deye, and Lee

Turkevich for their helpful comments on the manuscript. This research was supported in part by the National Toxicology Program (NTP) and NIOSH Nanotechnology Research Center (NTRC) Program (93908N0).

Disclaimer

The mention of any company or product does not constitute an endorsement by the Centers for Disease Control and Prevention. The findings and conclusions in this paper are those of the authors and do not necessarily represent the views of the National Institute for Occupational Safety and Health.

Appendix A. Supporting information

Supplementary data associated with this article can be found in the online version at doi:10.1016/j.jaerosci.2018.10.004.

References

Bach, S., & Schmidt, E. (2008). Determining the dustiness of powders–a comparison of three measuring devices. *Annals of Occupational Hygiene, 52*, 717–725.
Baron, P. A., Deye, G. J., Chen, B. T., Schwegler-Berry, D. E., Shvedova, A. A., & Castranova, V. (2008). Aerosolization of single-walled carbon nanotubes for an inhalation study. *Inhalation Toxicology, 20*, 751–760.
Baughman, R. H., Zakhidov, A. A., & de Heer, W. A. (2002). Carbon nanotubes - the route toward applications. *Science, 297*, 787–792.
Birch, M. E., Ku, B. K., Evans, D. E., & Ruda-Eberenz, T. A. (2011). Exposure and emissions monitoring during carbon nanofiber production-part I: elemental carbon and iron-soot aerosols. *Annals of Occupational Hygiene, 55*, 1016–1036.
Birch, M. E. et al. (2018). private communication.
Birch, M. E., Ruda-Eberenz, T. A., Chai, M., Andrews, R., & Hatfield, R. L. (2013). Properties that influence the specific surface areas of carbon nanotubes and nanofibers. *Annals of Occupational Hygiene, 57*, 1148–1166.
BSI Standards Publication (2013). *Workplace exposure - Measurement of the dustiness of bulk materials - Part 1: Requirements and choice of test methods.* The British Standards Institution (EN 15051-1:2013).
Evans, D. E., Ku, B. K., Birch, M. E., & Dunn, K. H. (2010). Aerosol monitoring during carbon nanofiber production: Mobile direct-reading sampling. *Annals of Occupational Hygiene, 52*, 9–21.
Evans, D. E., Turkevich, L. A., Roettgers, C. T., Deye, G. J., & Baron, P. A. (2013). Dustiness of fine and nanoscale powders. *The Annals of Occupational Hygiene, 57*, 261–277.
Hinds, W. C. (1999). *Aerosol technology: Properties, behavior, and measurement of airborne particles.* New York, USA: John Wiley & Sons.
Jensen, K. A., Koponen, I. K., Clausen, P. A., & Schneider, T. (2009). Dustiness behaviour of loose and compacted Bentonite and organoclay powders: What is the difference in exposure risk? *Journal of Nanoparticle Research, 11*, 133–146.
Ku, B. K., & Evans, D. E. (2012). Investigation of aerosol surface area estimation from number and mass concentration measurements: Particle density effect. *Aerosol Science and Technology, 46*, 473–484.
Ku, B. K., & Kulkarni, P. (2015). Measurement of transport properties of aerosolized nanomaterials. *Journal of Aerosol Science, 90*, 169–181.
Ku, B. K., Emery, M. S., Maynard, A. D., Stolzenburg, M. R., & McMurry, P. H. (2006). In situ structure characterization of airborne carbon nanofibres by a tandem mobility-mass analysis. *Nanotechnology, 17*, 3613–3621.
Ku, B. K. (2010). Determination of the ratio of diffusion charging-based surface area to geometric surface area for spherical particles in the size range of 100–900 nm. *Journal of Aerosol Science, 4*, 835–847.
Maynard, A. D., Baron, P. A., Foley, M., Shvedova, A. A., Kisin, E. R., & Castranova, V. (2004). Exposure to carbon nanotube material: Aerosol release during the handling of unrefined single-walled carbon nanotube material. *Journal of Toxicology and Environmental Health Part A, 67*, 87–107.
McKinney, W., Chen, B., & Frazer, D. (2009). Computer controlled multi-walled carbon nanotube inhalation exposure system. *Inhalation Toxicology, 21*, 1053–1061.
McMurry, P. H., Wang, X., Park, K., & Ehara, K. (2002). The relationship between mass and mobility for atmospheric particles: A new technique for measuring particle density. *Aerosol Science and Technology, 36*, 227–238.
NIOSH (2013). Occupational Exposure to Carbon Nanotubes and Nanofibers: Current Intelligence Bulletin 65 [DHHS (NIOSH) Publication No. 2013–2145]. 〈http://www.cdc.gov/niosh/docs/2013-145/pdfs/2013-145.pdf〉.
Park, K., Cao, F., Kittelson, D. B., & McMurry, P. H. (2003). Relationship between particle mass and mobility for diesel exhaust particles. *Environmental Science & Technology, 37*, 577–583.
Pensis, I., Mareels, J., Dahmann, D., & Mark, D. (2010). Comparative evaluation of the dustiness of industrial minerals according to European standard EN 15051, 2006. *Annals of Occupational Hygiene, 54*, 204–216.
Schmoll, L. H., Elzey, S., Grassian, V. H., & O'Shaughnessy, P. T. (2009). Nanoparticle aerosol generation methods from bulk powders for inhalation exposure studies. *Nanotoxicology, 3*(4), 265–275.
Schneider, T., & Jensen, K. A. (2008). Combined single-drop and rotating drum dustiness test of fine to nanosize powders using a small drum. *Annals of Occupational Hygiene, 52*, 23–34.
Stark, W. J., Stoessel, P. R., Wohlleben, W., & Hafner, A. (2015). Industrial applications of nanoparticles. *Chemical Society Reviews, 44*, 5793–5805.
Tsai, C. J., Wu, C. H., Leu, M. L., Chen, S. C., Huang, C. Y., Tsai, P. J., & Ko, F. H. (2009). Dustiness test of nanopowders using a standard rotating drum with a modified sampling train. *Journal of Nanoparticle Research, 11*(1), 121–131.
Weyel, D. A., Ellakkani, M., Alarie, Y., & Karol, M. (1984). An aerosol generator for the resuspension of cotton dust. *Toxicology and Applied Pharmacology, 76*, 544–547.
WHO document QAS/11.450 FINAL (2012). Bulk Density and Tapped Density of Powders.
Zhang, L., Aboagye, A., Kelkar, A., Lai, C., & Fong, H. (2014). A review: Carbon nanofibers from electrospun polyacrylonitrile and their applications. *Journal of Materials Science, 49*, 463–480.
Zhao, Q. (2013). *Characterization and thermal decomposition behavior of carbon nanotubes and nanocomposites (Master Thesis).* School of Energy, Environmental, Biological and Medical Engineering, University of Cincinnati.